Development of a robust multiphase flow solver on general meshes; application to sodium boiling at the subchannel scale

Antoine Gerschenfeld, Yannick Gorsse

▶ **To cite this version:**

Antoine Gerschenfeld, Yannick Gorsse. Development of a robust multiphase flow solver on general meshes; application to sodium boiling at the subchannel scale. NURETH-19 - 19th International Topical Meeting on Nuclear Reactor Thermal Hydraulics, Mar 2022, Bruxelles (virtuel), Belgium. cea-04439318

HAL Id: cea-04439318
https://cea.hal.science/cea-04439318v1

Submitted on 5 Feb 2024

HAL is a multi-disciplinary open access archive for the deposit and dissemination of scientific research documents, whether they are published or not. The documents may come from teaching and research institutions in France or abroad, or from public or private research centers.

L'archive ouverte pluridisciplinaire **HAL**, est destinée au dépôt et à la diffusion de documents scientifiques de niveau recherche, publiés ou non, émanant des établissements d'enseignement et de recherche français ou étrangers, des laboratoires publics ou privés.

DEVELOPMENT OF A ROBUST MULTIPHASE FLOW SOLVER ON GENERAL MESHES; APPLICATION TO SODIUM BOILING AT THE SUBCHANNEL SCALE

Antoine Gerschenfeld and Yannick Gorsse
DES - Service de Thermohydraulique et de Mécanique des Fluides (STMF)
CEA, Université Paris-Saclay, F-91191 Gif-sur-Yvette, France
antoine.gerschenfeld@cea.fr; yannick.gorsse@cea.fr

ABSTRACT

Euler-Euler simulations of two-phase flows, such as the 6-equations model adopted in many system thermal-hydraulics (STH) codes, becomes more challenging as the gas-liquid density ratio ρ_l/ρ_g increases. On structured meshes, the association of a staggered "MAC" numerical scheme with a semi-implicit "ICE" solution algorithm has proven particularly robust, and is currently used in the 3D modules of the TRACE, CATHARE or RELAP codes.

However, structured meshes are too restrictive to cover a number of potential applications : apart from the CFD scale, unstructured, polyhedral meshes are also encountered at the component scale when modelling SFR subassemblies. This later case is the focus of the TrioMC code developed at CEA. In 2019, this code was reimplemented using a new numerical scheme ("PolyMAC") designed to generalise to arbitrary meshes the main properties of the MAC staggered numerical scheme [1]. In 2020-2021, this scheme, originally designed to solve the single-phase Navier-Stokes and energy equations, was extended to multiphase flows: physical models dedicated to sodium boiling were then implemented in TrioMC, and preliminary validation was carried out against a benchmark sodium boiling test (the KNS-37 L22 test provided by the ESFR-SMART H2020 project).

KEYWORDS
numerical scheme, subchannel, multiphase, SFR, sodium boiling

Introduction

Contemporary Sodium Fast Reactor (SFR) oxide core designs, such as ASTRID or BN-1200, incorporate measures to lower the void reactivity effect of the core so that sodium boiling in the core does not lead to a power excursion. This constitutes a major safety innovation, as it should avoid the progression of Unprotected Loss-Of Flow (ULOF) transients to core degradation. From a modelling point of view, it presents a major challenge, requiring improvements both in the thermal-hydraulics of boiling sodium flows and in its coupling to the neutronics of the core.

On the thermal-hydraulics side, major efforts have been directed to adapting system thermal-hydraulics codes, such as TRACE or CATHARE, to boiling sodium flows. System-scale models of SFR cores represent individual or average subassemblies as a 1D mesh : this multi-1D approach remains can be performed on a single PC. By contrast, subchannel-scale simulations of complete SFR cores typically require HPC resources, while CFD simulations remain a challenge even for a single subassembly.

However, although they are impractical at the full-core scale, finer two-phase simulations can play a strong role in the design and interpretation of experiments. Due to practical constraints, subassembly boiling sodium tests must be performed at a reduced horizontal scale compared to reactor S/As (1-3 rings vs 8-10 in reactor S/As): at this small size, experimental behaviour tends to be affected by 3D effects (such as local boiling around the central pins). Since they simulate such effects, 3D codes can be used to analyse the scaling from reduced to reactor-scale. Similarly, when designing a new experiment, 3D pre-calculations can be used to position thermocouples at potential locations of interest: this is especially important in wire-wrapped bundles, where the total number of in-bundle is often limited (one in each wire and 4-6 per pin).

The current state-of-the-art for "finer than 1D" boiling sodium simulations can be summarized as follows:

- at the CFD scale, single-pin and 19-pin experiments have been simulated with Neptune_CFD;
- at the subchannel scale, several codes were developed in the 1980s such as CAFCA, SABRE or SABENA. Among those, SABENA was used as recently as 2006.
- finally, a number of 2D (r, z) or coarse 3D (r, θ, z) approaches have been developed, for instance as modules in the NATOF, SAS, ASTEC or SIMMER codes: more recently, such models have been developed in TRACE, COREMELT and OpenFOAM.

Because the liquid-gas density ratio of boiling sodium is particularly high ($\rho_l/\rho_g \sim 2000$) and because its high liquid thermal conductivity leads to fast vaporization, most of the codes cited above employ the staggered "MAC" numerical scheme together with the semi-implicit "ICE" time scheme in order to solve 4 to 6-equations models.

These choices explain the relative rarity of subchannel codes : the subchannel mesh for an SFR bundle (a mixture of triangular, rectangular and quadrangular prisms, see fig. X) is not compatible with the standard MAC scheme. [,,] implement a staggered scheme "by hand", by constructing specific interpolations for each mesh type : however, this approach is tedious and hard to generalize to complex subassemblies (fig. X). Transitions to free regions (such as sodium plena above the pin bundle) can also pose difficulties.

The TrioMC code, developed at CEA on the basis of the TRUST platform to model SFR subchannel thermal-hydraulics, initially adopted this approach. However, the need to model more complex S/As (such as fig. X) motivated a reimplementation of the code along the following lines:

1. a new numerical scheme ("PolyMAC"), conserving the main aspect of the MAC scheme but applicable to general polyhedra, was implemented in the TRUST platform;
2. source terms implementing physical models (pressure drop, wire mixing effects) and structures (pin conduction and fluid heating) were added to TrioMC.

The resulting implementation of TrioMC is equivalent to a traditional subchannel code, but could more accurately be described as a "coarse-grid CFD" code. Its structure easily allows for "unified subchannel-CFD" simulations, where subchannel correlations are only applied in the part of a domain where pin bundles are present, while turbulence models are applied in free areas. This strategy was used to model the primary vessel of the FFTF reactor for the IAEA CRP [], coupling it to CATHARE using the MATHYS coupling tool.

Efforts to extend TrioMC to two-phase flows began in 2020. Developments proceeded along the following steps, which also correspond to the structure of this paper:

1. a new architecture ("Pb_Multiphase") was implemented in the TRUST platform to describe generic N-phase flows using a $3N$-equation system, along with the ICE (semi-implicit) and SETS (prediction-correction) time schemes;
2. in the course of this development, it became apparent that some features of the PolyMAC numerical scheme would prevent an efficient implementation of the ICE time scheme. To solve this issue, a modified scheme (PolyMAC V2) was designed and implemented in TRUST;
3. the resulting multiphase solver was evaluated on a benchmark sedimentation test case;
4. source terms implementing physical models suitable for sodium boiling were implemented in TRUST and/or TrioMC;
5. the resulting two-phase sodium subchannel model was validated against a sodium boiling test : a loss-of-flow test at constant power performed on the KNS-37 37-pin sodium loop at KfK/KIT. Data for this test (L22) was provided to CEA as part of a benchmark conducted within the ESFR-SMART H2020 project.

These five sections are concluded by an outline of potential future developments.

1. Architecture for multiphase flows in the trust platform

The TRUST platform offers a flexible architecture where the user can specify one or more "problems" consisting each in one or more "equations": for instance, the `Pb_Thermohydraulique` problem describes a single-phase incompressible fluid through a `Navier_Stokes_std` equation for the velocity/pressure $(p, \vec{v})$ and a `Convection_Diffusion_Temperature` equation for the temperature T. Default classes implement heat conduction problems as well as incompressible and quasi-compressible (thermal-)hydraulics; additional classes incorporating turbulence models are implemented in the TRUST-based TrioCFD code. Aside from its equations, each problem is associated with a *medium* class (describing its medium properties), a *discretization* class (describing how the equations should be discretized in space), and a *time scheme* class (describing how its equations should be integrated in time).

In order to describe multiphase flows, we implemented a new `Pb_Multiphase` class describing the following equations:

$$\frac{\partial \alpha_k \rho_k}{\partial t} + \nabla.(\alpha_k \rho_k \vec{v}_k) = \sum_{l \neq k} \Gamma_{kl} \qquad (\mathcal{M}_k)$$

$$\alpha_k \rho_k \frac{\partial \vec{v}_k}{\partial t} + \nabla.(\alpha_k \rho_k \vec{v}_k \otimes \vec{v}_k) - \vec{v}_k \nabla.(\alpha_k \rho_k \vec{v}_k) = -\alpha_k \nabla p + \nabla.(\alpha_k \mu_k (\nabla \vec{v}_k + {}^t \nabla \vec{v}_k)) + \sum_{l \neq k} \vec{F}^i_{kl} + \vec{F}^w_k \qquad (\mathcal{Q}_k)$$

$$\frac{\partial \alpha_k \rho_k e_k}{\partial t} + \nabla.(\alpha_k \rho_k e_k \vec{v}_k) = -p \left(\frac{\partial \alpha_k}{\partial t} + \nabla.(\alpha_k \vec{v}_k) \right) + \nabla.(\alpha_k \lambda_k \nabla T_k) + \sum_{l \neq k} (q^i_{kl} + \Gamma_{kl} h_k) + q^w_k \qquad (\mathcal{E}_k)$$

The primary unknowns of this system are the volumetric fractions $(\alpha_k)_{1 \leq k \leq N}$, the phase velocities $\vec{v}_k$, the phase temperatures T_k and the (common) pressure p : the associated medium specifies the densities $\rho_k(p, T_k)$, internal energies $e(p, T_k)$ and enthalpies $h_k(p, T_k)$, viscosities $\mu_k(p, T_k)$ and thermal conductivities $\lambda_k(p, T_k)$. Physical models prescribe the momentum and heat transfers from phase k to the (k, l) interface ($\vec{F}^i_{kl}$, q^i_{kl}) and to the wall ($\vec{F}^w_k$, q^w_k), while interface jump conditions lead to $\Gamma_{kl} = -\Gamma_{lk} = (q^i_{kl} + q^i_{lk})/(h_l - h_k)$ and $\vec{F}^i_{lk} = -\vec{F}^i_{kl}$. The system is finally closed by the continuity condition $\sum \alpha_k = 1$. Implementation aspects led to the choice of a semi-conservative form for the momentum equations $\mathcal{Q}$ (to avoid terms proportional to Γ_{kl}) and to the choice of an internal energy equation for $\mathcal{E}$ (to avoid additional terms for each force in $\mathcal{Q}$).

The system ($\mathcal{M}$, $\mathcal{Q}$, $\mathcal{E}$) is in most cases nonlinear and tightly coupled by its source terms Γ_{kl}, $\vec{F}^i_{kl}$ and q^i_{kl}: the ICE time scheme offers a way to integrate these terms implicitly while avoiding the solution of a full linear system in $(\alpha, \vec{v}, T, p)$. It consists in the following choice of implicit terms (in red) :

$$\frac{\partial \alpha_k \rho_k}{\partial t} + \nabla.(\alpha_k \rho_k \vec{v}_k) = \sum_{l \neq k} \Gamma_{kl}$$

$$\alpha_k \rho_k \frac{\partial \vec{v}_k}{\partial t} + \nabla.(\alpha_k \rho_k \vec{v}_k \otimes \vec{v}_k) - \vec{v}_k \nabla.(\alpha_k \rho_k \vec{v}_k) = -\alpha_k \nabla p + \nabla.(\alpha_k \mu_k (\nabla \vec{v}_k + {}^t \nabla \vec{v}_k)) + \sum_{l \neq k} \vec{F}^i_{kl} + \vec{F}^w_k$$

$$\frac{\partial \alpha_k \rho_k e_k}{\partial t} + \nabla.(\alpha_k \rho_k e_k \vec{v}_k) = -p \left(\frac{\partial \alpha_k}{\partial t} + \nabla.(\alpha_k \vec{v}_k) \right) + \nabla.(\alpha_k \lambda_k \nabla T_k) + \sum_{l \neq k} (q^i_{kl} + \Gamma_{kl} h_k) + q^w_k$$

Under this form, linearizing each equation E for a given increment $(\delta\alpha, \delta\vec{v}, \delta T, \delta p)$ of the primary variables as $\delta E = \frac{\partial E}{\partial \alpha}.\delta\alpha + \frac{\partial E}{\partial \vec{v}}.\delta\vec{v} + \frac{\partial E}{\partial T}.\delta T + \frac{\partial E}{\partial p}.\delta p$ leads to a linear system of the form

$$\begin{pmatrix} \frac{\partial \mathcal{M}}{\partial \alpha} & \frac{\partial \mathcal{M}}{\partial T} & \frac{\partial \mathcal{M}}{\partial \vec{v}} & \frac{\partial \mathcal{M}}{\partial p} \\ \frac{\partial \mathcal{E}}{\partial \alpha} & \frac{\partial \mathcal{E}}{\partial T} & \frac{\partial \mathcal{E}}{\partial \vec{v}} & \frac{\partial \mathcal{E}}{\partial p} \\ 0 & 0 & \frac{\partial \mathcal{Q}}{\partial \vec{v}} & \frac{\partial \mathcal{Q}}{\partial p} \end{pmatrix} . \begin{pmatrix} \delta\alpha \\ \delta T \\ \delta\vec{v} \\ \delta p \end{pmatrix} = \begin{pmatrix} \delta\mathcal{M} \\ \delta\mathcal{E} \\ \delta\mathcal{Q} \end{pmatrix}, \tag{1}$$

where the blue and green blocks are purely "local" : when the equations are discretized (for instance via the PolyMAC scheme), these blocks only contain non-zero terms for lines and columns belonging to the same mesh location. They can thus be inverted as a series of local linear systems ((N, N) for the green block and $(2N, 2N)$ for the blue block) : since the overall system is upper-triangular, it can thus be inverted as $\delta\alpha = \delta\alpha^0 + M_\alpha \delta p$, $\delta\vec{v} = \delta\vec{v}^0 + M_{\vec{v}} \delta p$ and $\delta T = \delta T^0 + M_T \delta p$. Inserting the first relationship into the continuity constraint $\sum \alpha_k = 0$ leads to a system involving only the pressure increments δp : this system can then be solved at each step of a Newton algorithm for the complete nonlinear system.

Compared to a full system over the increments $(\alpha, \vec{v}, T, p)$, this reduced system offers several advantages:

- it is vastly smaller (by a factor of around $8N + 1$ in 3D) and does not increase in size for a larger number of phases;
- its structure is in most cases elliptic (it resembles those of a discretized Poisson equation), and can thus be solved efficiently at large scale and/or in parallel by multigrid methods.

On the other hand, the explicit discretization of convected quantities in (1) means that convective instabilities for time steps above the material Courant-Friedrich-Levy (CFL) limit. In order to overcome this limit, additional predictor steps can be implemented to provide initial estimates of these convected quantities: this scheme, known as SETS, was implemented and found to vastly improve timesteps when the transient dynamics are slow.

In order to implement the ICE scheme, the underlying architecture must be capable of providing the sparse matrices corresponding to each block of the Jacobian (1). In TRUST, this computation is spread between the space discretization, equation and medium classes in order to maximize code reuse. For instance, the derivative of the convective term of the mass equation $\mathcal{M}_k$ w.r.t. the phase temperature T_k is computed as :

$$\frac{\partial \nabla.(\alpha_k \rho_k \vec{v}_k)}{\partial T_k} = \frac{\partial \nabla.(\alpha_k \rho_k \vec{v}_k)}{\partial \alpha_k \rho_k} . \frac{\partial \alpha_k \rho_k}{\partial \rho_k} . \frac{\partial \rho_k}{\partial T_k}$$

where :

- the red term is computed by the convection operator of the underlying space discretization, such as PolyMAC. This operator implements a term of the form $\nabla.(F\vec{v})$ for a convected field F : the instance of this term associated with $\mathcal{M}_k$ operates with $F = \alpha_k\rho_k$, while another instance associated to $\mathcal{E}_k$ operates with $F = \alpha_k\rho_k e_k$. Both equations rely on the same code to compute the matrix $\partial\nabla.(F\vec{v})/\partial F$;
- the green term $\partial\alpha_k\rho_k/\partial\rho_k$ is local, and computed by the equation $\mathcal{M}_k$ where the field $F = \alpha_k\rho_k$ is defined. This field relies on the fields α_k (a primary unknown) and ρ_k (the density, provided by the medium);
- finally, the blue term is computed by the medium associated to the problem, where the density field $\rho_k(p, T_k)$ is defined.

This architecture has been designed to maximize code reuse, in particular at the level of the underlying space discretization. It has been found to be flexible and efficient : for instance, for single-phase subassembly calculations in TrioMC, a SETS multiphase problem with $N = 1$ is only $\sim 25\%$ slower than the incompressible Navier-Stokes resolution normally used in this case.

The $3N$-equation system $(\mathcal{M}_k, \mathcal{Q}_k, \mathcal{E}_k)$ presents particular difficulties in the case of a vanishing phase, $\alpha_k \to 0$. In the CATHARE code, this issue is handled by defining "residual" void fractions $\alpha_l^{res} = 10^{-6}$ and $\alpha_g^{res} = 10^{-5}$ and by introducing a term Γ_{kl}^{res} in the equations which strongly drives α_k to α_k^{res} when $\alpha_k < \alpha_k^{res}$: if a Newton iteration leads to $\alpha_k < 0$, the solution algorithm is aborted and the time step is reduced. In `Pb_Multiphase`, no residual void fraction is used : rather, a limiter is placed on the total phase change $\Gamma_k = \sum_l \Gamma_{kl}$. For a time step Δt, The time-discretized form of the mass equation $\mathcal{M}_k$ reads

$$\frac{\alpha_k^+\rho_k^+ - \alpha_k^-\rho_k^-}{\Delta t} + \nabla.(\alpha_k\rho_k\vec{v}_k) = \Gamma_k$$

with the -/+ superscripts denoting values at times t and $t + \Delta t$: hence, the condition $\alpha_k^+ \geq 0$ leads to

$$\Gamma_k \geq \Gamma_k^{lim} = \nabla.(\alpha_k\rho_k\vec{v}_k) - \frac{\alpha_k^-\rho_k^-}{\Delta t}\,.$$

At a given iteration, if $\Gamma_k < \Gamma_k^{lim}$, then the mass flux Γ_{kl} to the "dominant" phase l (those with the highest α_l) is modified so that $\Gamma_k = \Gamma_k^{lim}$: finally, the heat flux from phase l, q_{lk}^i, is modified so that the jump condition $\Gamma_{kl} = (q_{kl}^i + q_{lk}^i)/(h_l - h_k)$ is preserved. This process ensures that the converged solution of the Newton algorithm will satisfy $\alpha_k \geq 0$ while maintaining consistent mass, energy and momentum balances between the phases. Intermediate iterations may still lead to $\alpha_k^+ < 0$: thus, at the end of each iteration, the α_k must be post-processed to ensure $\alpha_k = 0$ while preserving $\sum \alpha_k = 1$. Final convergence is only declared once the algorithm converges to a solution satisfying $\alpha_k \geq 0$.

Additionally, the momentum and energy equations must ensure that $\vec{v}_k \to \vec{v}_l$ and $T_k \to T_{sat}$ when $\alpha_k \to 0$. In `Pb_Multiphase`, this is obtained by ensuring that the interfacial exchange terms $\vec{F}_{kl}^i$ and q_{kl}^i converge to $\varepsilon(\vec{v}_k - \vec{v}_l)$ and $\varepsilon(T_k - T_{sat})$ as $\alpha_k \to 0$.

2. The PolyMAC V2 numerical scheme

The architecture described in Section 1 is largely independant from the underlying numerical scheme: it can, for instance, be run "out-of-box" on the MAC numerical scheme for Cartesian meshes implemented in the TRUST platform. However, target meshes (fig. X) can only be treated by the PolyMAC scheme.

In its initial version [1], PolyMAC discretizes the incompressible Navier-Stokes equation under the form

$$\partial_t \vec{v} + (\vec{v}.\nabla)\vec{v} = -\nabla p - \nu \nabla \wedge (\nabla \wedge \vec{v}) \tag{2}$$

and leads to an irreductible, saddle-point linear system over the variables $(p, \vec{v})$ even when employing a predictor-corrector solution method such as SIMPLE or PISO : in that case, the linear system for the correction step reads

$$\begin{pmatrix} H_2 & G \\ -D & 0 \end{pmatrix} . \begin{pmatrix} \delta v \\ \Delta t \delta p \end{pmatrix} = \begin{pmatrix} 0 \\ -Dv^* \end{pmatrix}$$

with $v*$ the velocity computed by the prediction step, G and D the gradient and divergence operators (related by $D = -G^t$), and H_2 a symmetric, positive definite matrix. While this matrix is SPD, its saddle-point structure prevent its easy solution by multigrid methods: furthermore, its coupled structure means that, in a multiphase problem, systems with a velocity unknown per phase $\vec{v}_k$ but a single pressure unknown p will be hard to implement. Finally, the identity $\nabla.(\nu(\nabla\vec{v} +^t \nabla\vec{v})) = -\nu\nabla \wedge (\nabla \wedge \vec{v})$ used in (2) only holds for an incompressible fluid with constant viscosity : both assumptions are violated in the momentum diffusion term in $\mathcal{Q}_k$.

In order to solve these issues, a new version of the PolyMAC scheme ("PolyMAC V2") was developed and implemented in TRUST. As in PolyMAC, PolyMAC V2 represents the scalar variables (α, T, p) by their cell averages, noted $[\alpha]_c$ for a cell $c \in C$; on the other hand, velocities are represented by their face normal averages $[v]_f = \frac{1}{|f|}\int_f \vec{n}_f.\vec{v}.dS$, with $|f|$ and $\vec{n}_f$ the surface and normal of a face $f \in F$.
The discretization of the multiphase system $(\mathcal{M}_k, \mathcal{Q}_k, \mathcal{E}_k)$ is performed in three steps :

- discretization of the face gradient $[\Lambda\nabla u]_f$ of a scalar variable u (discrettized by $[u]_C = ([u]_c)_{c\in C}$) with Λ an arbitrary symmetric tensor;
- discretization of the scalar equations $\mathcal{M}_k$ and $\mathcal{E}_k$;
- discretization of the vector equation $\mathcal{Q}_k$.

2.1. Face discretization of gradients of scalar variables

The problem of constructing a face gradient $[\Lambda\nabla u]_f$ from cell averages $[u]_c$ has been widely studied in the context of simulating the anisotropic diffusion problem

$$\nabla.(\Lambda\nabla u) = f\,. \tag{3}$$

Among the many schemes developed for solving (3), cell-centered, flux-based schemes can be used to construct a face gradient suitable for PolyMAC V2. Two such schemes present particularly attractive properties:

- the gradient of [X] leads to a convergent, unconditionally stable scheme on general polyhedral meshes. On the reverse, its stencil can be quite large, extending to cells sharing a face with each neighbor of face f;
- the scheme defined in [Y] offers the same properties with a smaller stencil (limited to cells sharing a vertex with face f), provided that the mesh si such that, for each face f, the line connecting the cell centers on each side of f intersects the face. Expressions for the face gradients associated with this scheme were computed in [Z].

PolyMAC V2 consists in a hybrid approach between these two schemes, implementing the small-stencil gradient of [Y] where it can be applied and falling back to the large-stencil gradient of [X] otherwise. This ensures, in particular, that the elliptic part of the reduced pressure system produced by the ICE scheme will be symmetric, positive and definite on any mesh.

2.2. Discretization of scalar equations

Given that the velocity field $\vec{v}$ is discretized by its face normals, convective terms of the form $\nabla.(F\vec{v})$, with F a scalar field, can be easily discretized as

$$[\nabla.(F\vec{v})]_c = \frac{1}{|c|}\sum_{f\in F_c} |f|[F]_f[v]_{cf}\,, \tag{4}$$

with $|c|$ the volume of cell c, F_c the set of its faces, $[v]_{cf} = \pm[v]_f$ the normal velocity outgoing from c, and $[F]_f$ a face reconstruction of F at f from its values on each side of f : a simple upwind reconstruction is currently used in PolyMAC V2. This method is used to discretize the term $\nabla.(\alpha_k\rho_k\vec{v}_k)$ in $\mathcal{M}_k$ and the terms $\nabla.(\alpha_k\rho_k e_k\vec{v}_k)$, $\nabla.(\alpha_k\vec{v}_k)$ in $\mathcal{E}_k$.

The gradient discretization approach described in §2.1 is used to discretize the heat conduction term $\nabla.(\alpha_k\lambda_k\nabla T_k)$ in the energy equation $\mathcal{E}_k$, by taking $\Lambda = \alpha_k\lambda_k I$ to obtain $[\alpha_k\lambda_k\nabla T_k]_f$: then, its divergence can be easily obtained by $[\nabla.\vec{v}]_c = \frac{1}{|c|}\sum_{f\in F_c}[v]_{cf}$.

Finally, all the remaining terms in $\mathcal{M}_k$ and $\mathcal{E}_k$ are simply evaluated at cell c. When encountering a vanishing phase, the phase change terms Γ_{kl} and the interfacial heat flux q^i_{kl} may depend on the neighboring face velocities through the term $\nabla.(\alpha_k\rho_k\vec{v}_k)$ in Γ^{lim}_k : physical models may also depend on phase velocities within each cells. These are calculated using the following interpolation of the velocity vector:

$$[\vec{v}]_c = \frac{1}{|c|}\sum_{f\in F_c} |f|[v]_{cf}(\vec{x}_f - \vec{x}_c)\,, \tag{5}$$

where $\vec{x}_f$ and $\vec{x}_c$ are the respective barycenters of face f and cell c.

2.3. Discretization of the momentum equation

Since the phase velocities $\vec{v}_k$ are discretized by their face normals, the momentum equation $\mathcal{Q}_k$ should itself be discretized in the same way. However, constructing operators such as $[\nabla.(\alpha_k\rho_k\vec{v}_k\otimes\vec{v}_k)]_f$ and $[\nabla.(\alpha_k\mu_k\nabla\vec{v}_k)]_f$ directly from the face normal velocities $[v_k]_f$ presents a major challenge on polyhedral grids. For these operators, PolyMAC V2 extends a technique already used by PolyMAC for the convection operator :

1. reconstruct the phase velocity vectors in each cell at time t, $[\vec{v}_k^{-}]_c$, by (5);
2. Discretize the momentum equation at cells, by using (4) for each part of the convective term and a face gradient discretization of $[\vec{v}_k]_c$ (§2.1) with $\Lambda = \alpha_k\mu_k I$;
3. finally, discretize the momentum equation $\mathcal{Q}_k$ at faces by using, for the convective and diffusive terms, interpolations of the form

$$[\nabla.(\alpha_k\rho_k\vec{v}_k\otimes\vec{v}_k)]_f = \sum_{c\in C_f}\alpha_{fc}\vec{n}_f.[\nabla.(\alpha_k\rho_k\vec{v}_k\otimes\vec{v}_k)]_c$$

where $C_f = \{c, c'\}$ are the two cells neighboring c and where the coefficients α_{fc} are chosen so that $\sum \alpha_{fc} = 1$: in practice, the choice $\alpha_{fc} = \frac{d_{fc'}}{d_{fc}+d_{fc'}}$, corresponding to a harmonic average, gave best results. The pressure gradient term ∇p is obtained through a face discretization (as in §2.1) with $\Lambda = I$: the remaining terms are local, so that they can be evaluated directly at face f.

If the convection and diffusion operators must be treated implicitly (for instance as part of a predictor step), the cell and face velocity equations are solved simultaneously, in a linear system of the form

$$\begin{pmatrix} M_C & M_{FC} \\ 0 & M_F \end{pmatrix} \cdot \begin{pmatrix} [\delta\vec{v}]_C \\ [\delta v]_F \end{pmatrix} = \begin{pmatrix} [\delta\mathcal{Q}]_C \\ [\delta\mathcal{Q}]_F \end{pmatrix} ;$$

the bottom-left term of this matrix is null as the face equations depend on the cell velocities, but the cell equations do not depend on the face velocities. In a semi-implicit solution method such as ICE, the past time cell velocities $[\vec{v}_k^-]_c$ can be used directly when evaluating the convection and diffusion operators at the faces : hence, the cell equations do not need to be solved at all.

Because the face equations $[\mathcal{Q}_k]_F$ use a direct face discretization of the pressure gradient, this discretization offers the same pressure-velocity coupling as a completely staggered scheme: however, its convection and diffusion operators are the same as those of a collocated scheme. In single-phase, its stability and convergence properties have been checked against the FVCA8 benchmarks []. A similar approach has been explored in OpenFOAM, where it was observed to reduce checkerboard modes compared to a fully-collocated formulation [Wheeler, Radman]

3. Solver benchmarking on sedimentation test case

4. TrioMC physical models for sodium boiling

The initial reimplementation of TrioMC based on PolyMAC [1] implemented, as source terms, a number of physical models in order to model single-phase flows :

- in the momentum equations, the "uCTD" detailed Cheng-Todreas correlation in the axial direction [2] and the Gunther-Shaw correlation [3] in the transverse direction;
- in the energy equation, wall heat transfers based on the Seban-Shimazaki [4] Nusselt number correlation. These transfers occur both where the fluid is in contact with an explicitly-solid mesh (such as the hexagonal wrapper) and with immersed pins, which are not explicitly present in the fluid mesh. Internal conduction within each of these pins is modeled by a 3D, cylindrical coordinates heat conduction module;
- in both equations, diffusion coefficients are modified in the transverse direction in order to account for the tortuosity of the medium (which reduces diffusive transfers compared to the axial direction) and to account for mixing effects due to wire wrappers. In periheral channels, wires result in convective rather than in diffusive mixing: in these channels, the Gunter-Shaw transverse pressure drop correlation is modified to account for this "swirling" force.

In order to extend TrioMC to two-phase flows, these models must be complemented by a number of additional correlations. The choices below took as a starting point the SABENA code [5], with modification guided by experience accumulated at CEA over the validation of CATHARE [6] and BACCARAT [7]. The following models were implemented:

Flow pattern

Due to the high liquid-gas density ratio of sodium, the flow pattern is assumed to be purely annular : in practice, simulated void fractions rarely fall below $\alpha \sim 0.7$. Thus, the interfacial area A_i, as well as length scales associated with the liquid film (δ_l) and gas core (δ_g) can be estimated easily:

$$A_i = \frac{4\sqrt{\alpha_g}}{D_h} \, , \delta_l = \frac{D_h}{2}(1 - \sqrt{\alpha_g}) \, , \delta_g = D_h - 2\delta_l$$

with D_h the local hydraulic diameter.
Source: SABENA

Momentum transfers

Consistently with the assumption of annular flow, the Wallis interfacial friction correlation [8] is used for interfacial friction:

$$\vec{F}^i_{lg} = -\vec{F}^i_{gl} = -A_i C^i_f \rho_g ||\vec{v}_l - \vec{v}_g|| (\vec{v}_l - \vec{v}_g) \, , C_f = 5.10^{-3} \left[1 + 300\frac{\delta_l}{D_h}\right]$$

Source: SABENA
Wall friction is computed via a modified Muhler-Steinhagen-Heck [9] two-phase multiplier:

$$\vec{F}^w = -\frac{1}{2D_h}\frac{f_m}{\rho_m}||\vec{G}||\vec{G} \, , \frac{f_m}{\rho_m} = \left[\frac{f_l}{\rho_l} + 2\left(\frac{f_g}{\rho_g} - \frac{f_l}{\rho_l}\right)x^\beta\right](1-x)^{1/3} + \frac{f_g}{\rho_g}x^3$$

where $\vec{G} = \sum \alpha_k \rho_k \vec{v}_k$ is the total mass flux, x is the flow quality and f_l, f_g are single-phase friction factors obtained by assuming that then flow G is completely liquid or gaseous. The coefficient $\beta = 1.2$ was added in [7] to improve pressure drop predictions in the CEA GR19 experiment.
This wall friction acts entirely on the liquid phase ($\vec{F}^w_l = \vec{F}^w$, $\vec{F}^w_g = \vec{0}$) as long as $\alpha_l > 10^{-3}$, with a linear switch to $\vec{F}^w_g$ for $0 \leq \alpha_l \leq 10^{-3}$.
Source: BACCARAT

Heat transfers

Interfacial heat transfers on the liquid and gas side are computed by Nusselt number correlations:

$$q^i_{lg} = A_i \frac{\lambda_l}{\delta_l} Nu_l (T_{sat} - T_l) \, , q^i_{gl} = A_i \frac{\lambda_g}{\delta_g} Nu_g (T_{sat} - T_g) \tag{6}$$

where Nu_l and Nu_g are computed respectively by the Seban-Shimazaki [4] and Dittus-Boetler [10] correlations.
Similarly, wall heat exchanges are computed as

$$q^w_l = A_{wl} \frac{\lambda_l}{\delta_l} Nu_l (T_w - T_l) \, , q^w_g = A_{wg} \frac{\lambda_g}{\delta_g} Nu_g (T_w - T_g) \tag{7}$$

with A_{wl} and A_{wg} the volumetric wall area in contact with the liquid and gas phase. The liquid film is assumed to completely cover the walls ($A_{wl} = A_w$, $A_{wg} = 0$) until $\alpha_g = 0.975$: A_{wg} is then increased inearily with α_g until $\alpha_g = 0.99$, after which ($A_{wl} = 0$, $A_{wg} = A_w$).
Source : original

5. Validation on the KNS-37 L22 Test

The KNS "compact sodium boiling" loop was commissioned at KIT/KfK in the 1970s in support of sodium boiling studies in support of the SNR-300 reactor project [11]. Its 37-pin test section, KNS-37 (fig. 1), featured a 37-pin bundle with spacer grids : the electrically-heated pins could each provide up to 16KW with a cosine power profile. More than 100 boiling tests were performed on this test sections : among those, the L22 test, consisting in a loss-of-flow transient at constant power with a flow halving time of 2.35s, served as the reference test for two benchmarks [12] as well as for several validation studies [5]. It was thus a natural first choice for a first two-phase validation of TrioMC.

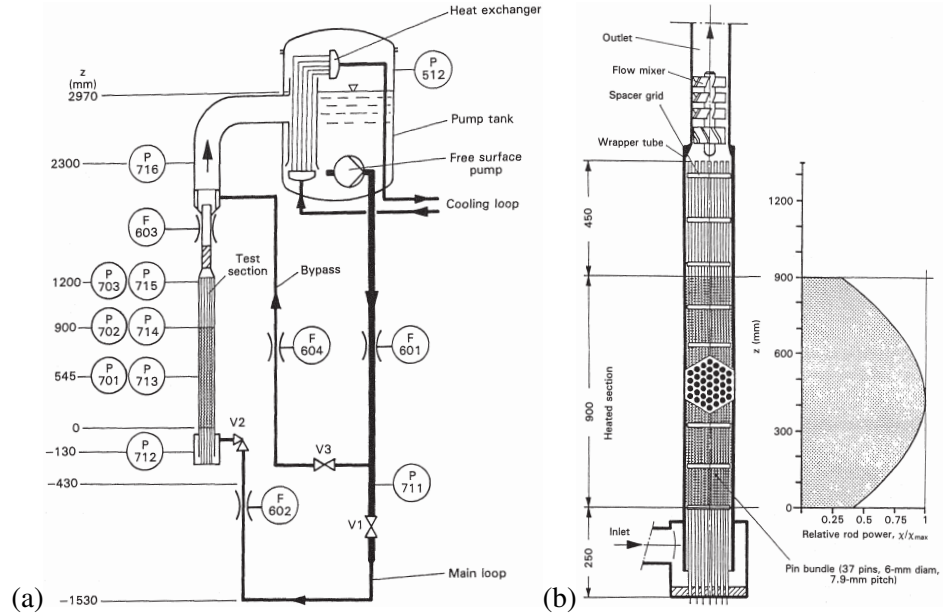

Figure 1. Overview of the KNS-37 experiment : loop (a), test section and power profile (b).

In order to reproduce the dynamic behavior associated with a transient test, the complete loop (fig. 1.a) should ideally be modelled, for instance coupling TrioMC to the CATHARE system code. As a temporary alternative, the main loop of the test section was modelled from the upstream pressure sensor P711 to the downstream pressure sensor P716, with imposed pressure boundary conditions provided by experimental measurements at these two locations: at low flow rates, this approximation is expected to be roughly equivalent to the real loop behavior, due to the presence of a bypass line between these two locations. Other boundary conditions include the test section inlet temperature (constant at $T = 379°$), the bundle power (713 KW) and heat losses at the outside of the hexcan (heat exchange at $h_{ext} = 6.7$ W/m^{2}K with an external temperature $T_{ext} = 40°$).

The TrioMC fluid domain uses a single radial mesh in the upstream region (from P711 to P712), the standard subchannel mesh in the bundle region (from P712 to P715), and an extrusion of the subchannel mesh in the downstream region (from P715 to P716), for a total of around 7236 meshes: it is coupled to a solid domain simulating the hexagonal wrapper. Calibration on the initial steady-state of the L22 tests led to a few changes in the TrioMC models (§4):

- thermal balance considerations provided a 5% lower power estimate compared to the theoretical value of 713 KW, as noticed in [11]. The thermal power input in the TrioMC model was thus

reduced by this amount;

- pressure signals P712, P713 and P714 indicated that the axial pressure drop in the test section was severely underestimated by the uCTD correlation, as the nine spacer grids (fig. 1b) were unaccounted for. A multiplicative factor of 2.3 was applied in order to recover the correct pressure drop;
- finally, analysis of the initial radial temperature profile showed that transverse heat transfers were underestimated as well, likely because the spacer grid led to mixing effects. A factor of 2 was applied to the transverse mixing coefficients to account for this effect.

The following phenomena occur over the L22 transient:

- boiling starts in the center subchannels at $t = 6.11$s;
- (A) from $t = 6.91$s, this boiling leads to high-frequency pressure/flowrate oscillations;

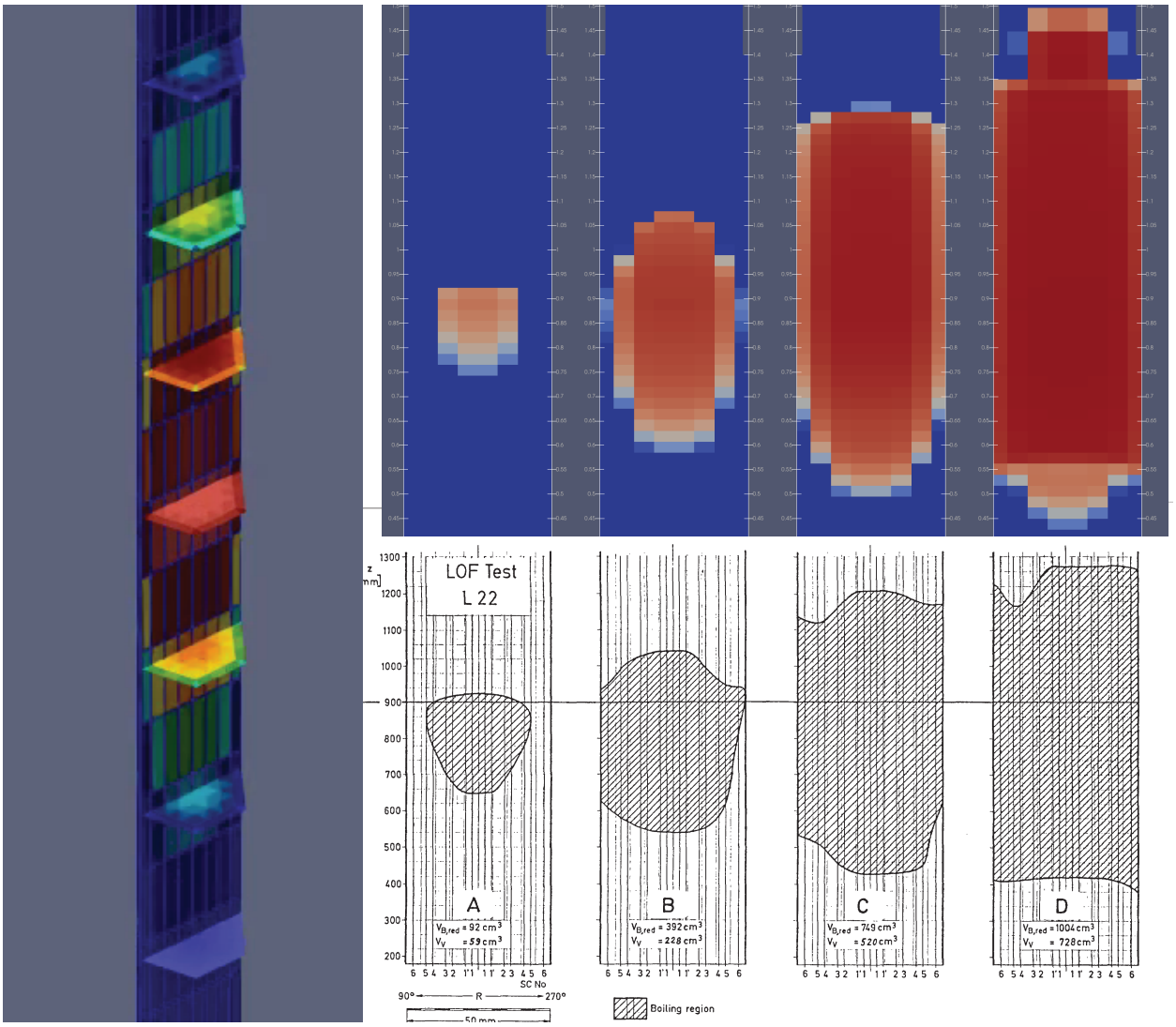

Figure 2. TrioMC simulation of the KNS-37 L22 test: subchannel mesh (left), comparison between calculated (top) and experimental (bottom) boiling regions at t = 6.91s (A), t = 9.31s (B), t = 9.25s (C) and t = 9.45s (D).

- (B) at $t = 8.31$s, boiling reaches the peripheral channels. This leads to the end of oscillatory behavior, as it is replaced by a rapid mass flow rate decrease (flow redistribution);
- (C) at $t = 9.25$s, pin wall temperatures in the central channels start to rise rapidly, indicating dryout;
- at $t = 9.45$s, a pin wall temperature reaches 950°, triggering a power shutoff to preserve the experiment;
- (D) vaporisation peaks at $t = 9.65$s, then condenses rapidly as the mass flowrate recovers.

The progression of the boiling region is broadly captured by the TrioMC simulation (fig. 2). Analysis of the mass flowrate and pressure signals (fig. 3a-b) shows that :

- in the radial expansion phase (A-B), overall flowrate and pressure trends are well predicted, although the oscillatory behavior in this phase is underestimated;
- in the axial expansion phase (B-D), flowrate and pressure trends are captured well;
- in the condensation phase after (D), the code predicts more recondensation at the top of the vapor region than observed in the experiment, leading to an underprediction of the outlet mass flowrate F603 and to the prediction of pressure peaks.

Analysis of the pin surface temperatures at two levels of the heated section (fig. 3c-d) shows that temperature evolutions before dryout are predicted well. The dryout itself is reproduced correctly in the center subchannels (T539 on fig.3c, T555 on fig.3d): howvever, the code also predicts a radial expansion of the dryout zone that is not born out experimentally. This indicates that the dryout criterion (the transition from $A_w l$ to A_{wg} in (7)) may require further work. It should be noted that the experimental dryout zone seems to be dissymetric (for instance, compare T550 and T554 in fig.3d).

Conclusion

The TrioMC SFR subchannel code was successfully extended to two-phase flows. This required the development of a multiphase solver in the underlying TRUST platform both applicable to general polyhedral meshes and robust enough to sustain the abrupt phenomena associated with boiling at high density ratios. This was achieved by generalizing the numerical strategy adopted by system codes. First, a flexible architecture for assembling the $3N$-equation system and solving it with the ICE scheme was first implemented in TRUST: then, the underlying PolyMAC numerical scheme was modified to satisfy the new requirements imposed by the architecture (in particular the ability to solve a single linear system on the pressure unknowns at each iteration).

Based on this developments, a first set of correlations was implemented in TrioMC (§4). Initial validation of the resulting 6-equations model on the KNS-37 L22 test (§5) showed encouraging results, but also led to the identification of several areas for improvement:

- radial expansion of the dryout region was overpredicted by the code, indicating that the simple dryout criterion by the wall heat transfer models (7) should be improved;
- the condensation phase following the power shut-off was considerably more violent in the calculation than observed experimentally : improvements to the interfacial heat transfer models (6) could solve this issue.

Overall, the L22 transient exhibits both high void fractions (with $\alpha_l < 1\%$) and high gas velocities (with v_g rising above 50m/s in the two-phase region). In this regime, entrainment of the liqudi film by the gas core is

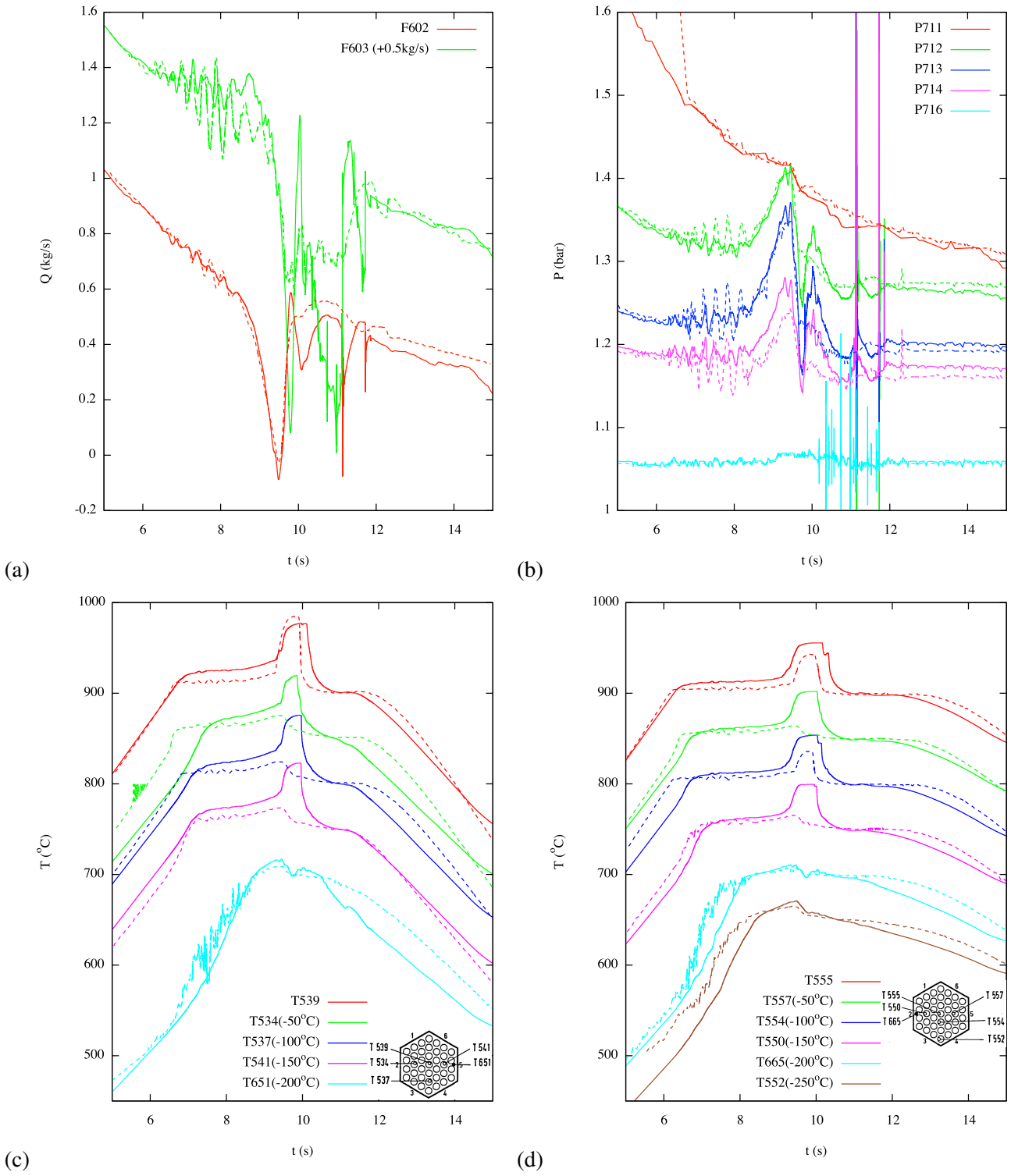

Figure 3. Comparison between simulation (plain lines) and experimental results (dots) for L22 test: (a) mass flowrates, (b) pressure signals, pin surface temperatures at (c) z = 720mm and (d) z = 870mm (see fig. 1.b).

expected to play a major role, resulting in particular in faster dryout at high gas velocities. In order to study this issue further, a three-field model (liquid film, droplets and gas) will be implemented in TrioMC: this approach was explored in SABENA [13] with promising results.

Aside from physical models, simulating the remaining parts of the KNS-37 loop (bypass line, pump and extension tanks) should also improve the prediction of dynamical aspects. For this purpose, the TrioMC model developed here will be coupled to the CATHARE model of the entire loop

References

[1] A. GERSCHENFELD, Y. GORSSE, and G. FAUCHET, "Development of a Polyhedral Staggered Mesh Scheme: Application to Subchannel and CFD SFR Thermal-Hydraulics," NURETH-18, 2019.

[2] S.-K. CHEN, Y. M. CHEN, and N. E. TODREAS, "The upgraded Cheng and Todreas correlation for pressure drop in hexagonal wire-wrapped rod bundles," *Nuclear Engineering and Design*, **335**, 356 (2018).

[3] A. Y. GUNTER and W. A. SHAW, "A general correlation of friction factors for various types of surfaces in cross flow," *Trans. ASME*, **67**, 643 (1945).

[4] R. SEBAN and T. SHIMAZAKI, "Heat Transfer to a Fluid Flowing Turbulently in a Smooth Tube with Walls at Constant Temperature," *Trans. ASME*, **73** (1949).

[5] H. NINOKATA and T. AKI OKANO, "SABENA: Subassembly boiling evolution numerical analysis," *Nuclear Engineering and Design*, **120**, *2–3*, 349 (1990).

[6] M. ANDERHUBER, J. PEREZ-MANES, and N. ALPY, "Validation of CATHARE-3 system code for sodium two-phase flow application : RD path and simulation of key-tests from SIENA program," *Proc. NURETH-17*, NURETH-17, 2017.

[7] E. BISSEN, *Semi-analytical methodology for stability and bifurcation analysis in a low pressure boiling channel for GEN4 SFR safety RD on two-phase flow limit cycles*, PhD thesis, 2019.

[8] G. B. WALLIS, *One-dimensional two-phase flow*, McGraw-Hill (1969).

[9] H. MULLER-STEINHAGEN and K. HECK, "A simple friction pressure drop correlation for two-phase flow in pipes," *Chemical Engineering and Processing: Process Intensification*, **20**, *6*, 297 (1986).

[10] F. DITTUS and L. BOELTER, "Heat transfer in automobile radiators of the tubular type," *International Communications in Heat and Mass Transfer*, **12**, *1*, 3 (1985).

[11] M. BOTTONI et al., "Experimental and Numerical Investigations of Sodium Boiling Experiments in Pin Bundle Geometry," *Nuclear Technology*, **89**, *1*, 56 (1990).

[12] H. KOTTOWSKI, *Liquid-Metal Thermal-Hydraulics*, Inforum Verl. (1995).

[13] H. NINOKATA and A. DEGUCHI, "Experimental validation of the subchannel two-fluid model code SABENA with out-of-pile sodium boiling experiments," *Proc. 4th International Topical Meeting on Nuclear Reactor Thermal Hydraulics,* (1989).